Ocean Dynamics (2004) ■■: 1–9
DOI 10.1007/s10236-004-0089-4

Georgy I. Shapiro · Johan van der Molen
Huib E. de Swart

The effect of velocity veering on sand transport in a shallow sea

Received: 31 October 2002 / Accepted: 05 January 2004

Abstract This study aims at comparing and contrasting two different models for sand transport by currents in a shallow sea to illustrate the effect of velocity veering. The first model uses the Bailard-type formulation, which allows calculation of erosion/deposition rates at a fixed location on the sea floor via the divergence of horizontal sediment fluxes. The second model is a semi-analytical 2.5-dimensional model, which takes into account the time lag between erosion and deposition events and the velocity veering within the sediment-laden (nepheloid) layer caused by the Coriolis force. The velocity veering implies that the direction of the sediment flux is generally different from the direction of the surface flow. The latter model was designed for rapid, semi-analytical computations of sediment transport, using flow fields from 2-DH numerical models. The two models use a matching set of parameters to provide identical values for the bottom stress and suspended sediment load for a uniform steady current at any given surface velocity. The two models were compared in a range of sand grain sizes 50–500 μm and current speeds up to 1 m s^{-1} for an idealised square region (100 × 100 km) of a shelf sea of constant depth. The erosion/deposition patterns and suspension load were examined in three settings: (1) uniform steady flow, (2) straight jet, (3) meandering jet. It was found that both the rates and, in particular, spatial distribution of the areas of erosion/deposition differ significantly between the models in cases (2) and (3). This difference can be attributed to additional flux divergence due to velocity veering. A comparison of model results with field data, collected at Long Island Shelf, supports the relevance of Coriolis-induced veering of currents on the direction of the sediment flux.

Keywords Sediment transport · Boundary layer · Ekman veering · Model · Shelf Seas

Responsible Editor: Jens Kappenberg

G. I. Shapiro (✉)[1]
Institute of Marine Studies, University of Plymouth,
Drake Circus, Plymouth, Devon PL4 8AA,
United Kingdom
e-mail: g.shapiro@plymouth.ac.uk

[1]Also at: P.P. Shirshov Institute of Oceanology,
Moscow, 117851, Russia

J. van der Molen
Institute for Marine and Atmospheric Research Utrecht (IMAU),
Utrecht University, Princetonplein 5,
3584 CC Utrecht, The Netherlands
e-mail: j.vandermolen@phys.uu.nl

H. E. de Swart
Institute for Marine and Atmospheric Research Utrecht (IMAU),
Utrecht University, Princetonplein 5,
3584 CC Utrecht, The Netherlands
e-mail: h.e.deswart@phys.uu.nl

1 Introduction

Understanding and predicting sand transport in shallow shelf seas is an important issue for scientists, coastal engineers and coastal zone management. At present, attention is not only on coastal waters but also on the shelf, because of the technical possibilities to build large engineering constructions there (artificial islands, wind parks), and to carry out large-scale sand mining. In energetic shelf seas with an erodible bottom, knowledge of the long-term morphodynamical development induced by such interventions is important, because these developments can potentially affect the long-term stability of the constructions themselves and/or (even more important) of the shelf sea coasts. In shelf seas, water depths are sufficiently large to allow the formation of an Ekman layer near the bottom as a result of the Coriolis force, which is characterised by changes in current direction and magnitude in the vertical. This effect was found to be significant for the transport of fine-grained sediment (Shapiro et al. 2000) in relatively deep shelf waters. Here, a first assessment is given of the influence of a bottom Ekman boundary layer on the magnitude and direction of the transport of sand, as well as on the resulting pattern of bed-level change and consequently

1 0 2 3 6 0 0 8 9 B
Journal number Manuscript number
Dispatch: 10.3.2004 Journal: Ocean Dynamics No. of pages: 9
Author's disk received ☑ Used ☑ Corrupted ☐ Mismatch ☐ Keyed ☐

on the initial trend of morphodynamical evolution in shallow coastal waters. The effect is expected to be important, because sand is typically transported close to the bottom, where the veering of the velocity with respect to the depth-averaged mean is maximal.

In the past decades a variety of formulations for sand transport under different hydrodynamic conditions has been developed (see e.g., Van Rijn 1993; Soulsby 1997 for overviews). They require knowledge of the shear stress acting at the sandy seabed. Nowadays, these formulations are implemented in many process-oriented morphodynamic models (see e.g. De Vriend et al. 1993; Nicholson et al. 1993; Nicholson et al. 1997 for overviews and model intercomparisons). Full 3-D hydrodynamical models (e.g. Backhaus and Hainbuches 1987) take into account various physical flow processes, including the Coriolis force, which acts on any moving particle because of Earth rotation. Since the practical applicability of full three-dimensional sediment-transport models is still in its infancy, it is common to use the models in a 2-D mode (see e.g. Gerritsen and Berentsen 1998; Van der Molen and de Swart 2001) with a prescribed vertical structure of the current (logarithmic profile) and without taking into account the veering of the velocity vector over the vertical. Besides, in the case of time-varying currents, also temporal phase differences between velocities at different vertical levels are neglected. Thus, in shallow areas with a sandy bottom and where currents experience veering over the vertical, such models yield incorrect magnitudes and directions of the sand transport. Consequently, deviations also occur in the computation of erosion and deposition areas of sediment, which are determined by the spatial divergence of the net sand flux.

For a first assessment of the effect of velocity veering, this study focuses on quasisteady currents (spatial scales >10 km, time scales >1 day) on the shelf (depths >10 m). Tidal situations are more complicated, because the variability in time prevents the full development of the Ekman layer. Instead, veering of the tidal ellipse occurs, together with phase differences in the vertical (Prandle 1982; Maas and Van Haren 1987). Tidal situations will be addressed in a subsequent paper.

Analysis of field data on the inner shelf near Long Island by Niedoroda and Swift (1991) demonstrate that already in depths of 15–30 m Ekman veering can be significant. Additional computations with a sand-transport model (which uses near-bed currents as input) suggest that depth-averaged currents and net sand fluxes have different directions. Field data on the Iberian shelf also reveal clear Ekman veering (Vitorino et al. 2002) with implications for the direction of transport of suspended matter (Oliveira et al. 2002). In very shallow basins, such as mixed estuaries and tidal basins with strong topographic control, Ekman veering usually is of minor importance.

The aim of the present work is to quantify the role of Ekman veering on both the sand-transport rates and the location of erosion/deposition areas on the continental shelf. The study is carried out by comparing two different models. The first model is based on the standard formulation of Bailard (1981) for suspended sand transport, which neglects velocity veering and a critical shear stress for erosion. Instead of Bailard's formulation, any other local suspended-load formulation could be used without affecting the conclusions of this study. The second is a new semi-analytical 2.5-dimensional boundary-layer model (Shapiro 2004), in which velocity veering due to Earth rotation is taken into account. The model is based on the sediment-transport model by Shapiro et al. (2000). The models were tuned to yield the same results for coarse sand and no Coriolis force.

The contents of this paper are as follows. In Section 2 the two different sand-transport models will be discussed. Results are shown in Section 3, followed by a discussion (Sect. 4) and the conclusions.

2 Sand-transport models

2.1 Bailard-type model

A sand-transport formulation (Van der Molen 2002) based on the original Bailard (1981) model is used here for the steady flow, because it is simple and based on the depth-integrated total sediment transport. This model predicts a fourth power dependence of the suspended transport upon a reference velocity defined at some height above the bottom. Bailard does not take into account the Coriolis force. Furthermore, the Bailard-type model uses a prescribed bottom roughness and assumes steady-state conditions (suspended particulate matter, hereafter called SPM, concentration is always in equilibrium with the current velocity) which implies that time-averaged velocity moments are involved in the consideration. It then calculates horizontal fluxes of suspended sediment at a fixed location, independently of the neighbouring points (one-point model) and preceding conditions (no memory). For an application of the Bailard formulation to compute sand transport in a shelf sea (North Sea), see Van der Molen (2002). Transport magnitudes computed with Bailard's formulation are comparable to field observations in shelf-sea conditions (Van der Molen 2003). The Bailard model operates with the depth-integrated horizontal SPM mass flux, q_s, which is calculated via the equation (see e.g. Soulsby 1997, p.180)

$$\mathbf{q}_s = \rho_s \frac{c_f \varepsilon_s}{g(s-1)w_s} |\mathbf{u}_a|^3 \mathbf{u}_a \ . \tag{1}$$

Here, $\mathbf{u}_a$ is the velocity vector at a fixed height a above the bottom, g is the acceleration due to gravity, s is the relative density of sand, ρ_s is the absolute sediment density, c_f is the friction factor, $\varepsilon_s = 0.02$ is the efficiency factor of suspended transport for steady current, w_s is the settling velocity of SPM and bold-faced variables are vectors. The specific value of ε_s is taken from the study by Van der Molen (2002) and represents a compromise

between the values of Bagnold (i.e. 0.01) and Bailard (0.025). The friction factor is given by

$$c_f = \frac{\kappa^2}{\ln^2\left(\frac{a}{z_0}\right)} \quad , \tag{2}$$

where $\kappa = 0.41$ is von Karman constant (Clauser 1956) and $z_0 = k_s/30$ is the roughness height, with k_s being the Nikuradse's bottom roughness.

In our computations, the hydrodynamic input consists of a given velocity $|\mathbf{u}_h|$ at the sea surface. To convert this to a near-bed velocity, $|\mathbf{u}_a|$, as used in Eq. (1), a logarithmic velocity profile (law of the wall) was assumed

$$|\mathbf{u}(z) = \frac{u_*}{\kappa}\ln\left(\frac{z}{z_0}\right) \quad u_* = \sqrt{c_f}|\mathbf{u_a}| \quad . \tag{3}$$

This choice means that possible veering of the velocity vector over vertical is not taken into account. In Eq. (3) u_* is the friction velocity at the seabed, which can be expressed via the surface current as

$$u_* = \frac{\kappa|\mathbf{u}_h|}{\ln\left(\frac{h}{z_0}\right)} \quad . \tag{4}$$

The near-bottom velocity, $|\mathbf{u}_a|$ is expressed via the surface current velocity, $|\mathbf{u}_h|$, using Eqs. (3) and (4).

The vertical SPM mass flux at the seabed, Q_v, is computed as a divergence of the horizontal mass flux:

$$Q_v = \frac{\partial q_{s,x}}{\partial x} + \frac{\partial q_{s,y}}{\partial y} \quad , \tag{5}$$

where subscripts x, y denote components of the horizontal mass flux q_s. This approach results in a so-called local equilibrium model.

Input parameters for the model are depth of water, h, surface current, $\mathbf{u}_h$, and SPM settling velocity, w_s.

Horizontal fluxes are obtained by applying Eqs. (1–4) at each location and then the vertical flux is computed via Eq. (5).

2.2 Velocity veering model

The 2.5-D model (Shapiro et al. 2000; G. I. Shapiro, personal communication, 2004) uses the vertical structure of current from a shallow-water version of the Ekman model rather than from the law of wall. For brevity, we call it the velocity veering SPM transport model (VVS). The VVS model has been developed for steady or slowly (subinertial frequency) varying currents. In the VVS model, the current velocity profile takes into account not only the variation of the value of current with height, but also of its direction. The result is that the direction of near-bottom current, which is the main agent in the transport of sand, deviates (generally) from the direction of both the surface and depth-averaged currents. This means that the direction of sand transport could be different from that of the total water flow. This deviation of the current constitutes the major difference between the VVS model and the Bailard-type or similar sand-transport models. While the hydrodynamic part of the VVS model mostly follows classical Ekman formulation (Pond and Pickard 2001), there is an important difference which has significant implications on suspended matter transport. The difference is that the present model has a vertical eddy viscosity (and diffusivity) coefficient that depends on the surface (or, alternatively, free stream) current velocity at each location, rather than assuming it to be a constant. This dependence is resolved using a mixing-length turbulence closure scheme, which gives an approximate expression for the turbulent friction and diffusion coefficients

$$K = \frac{2C_D^2|\overset{\mathrm{v}}{u_h}|^2 h}{2fh + C_D|\overset{\mathrm{v}}{u_h}|} \quad . \tag{6}$$

Here, f is the Coriolis parameter, and the drag coefficient C_D is defined such that $u_*^2 = C_D|\mathbf{u}_h|^2$.

The VVS model uses a prescribed drag coefficient, typically $C_D = (1\text{–}3) \times 10^{-3}$, to calculate both turbulent viscosity and diffusivity coefficients at each grid point, given the velocity of the surface current. The actual value of C_D can be taken as constant over the whole domain or be spatially variable and computed at each grid point from other known values, such as bottom roughness and water depth, using equations presented by Soulsby (1997), Sect. 3.3. Earth rotation and friction result in changes of both the magnitude and the direction of the current with depth. The vertical concentration profiles are also calculated at each grid point, given the current velocity and SPM settling velocity. These profiles are calculated using a local sediment entrainment–deposition balance at each location as a first approximation, which is then corrected by taking into account horizontal advection of sand in suspended state (G. I. Shapiro, personal communication, 2004).

The model calculates the SPM load, m, and the horizontal SPM mass flux, $\mathbf{Q}$, from

$$\frac{\partial m}{\partial t} + \frac{\partial Q_x}{\partial x} + \frac{\partial Q_y}{\partial y} = E - \frac{w_s m}{h_d \gamma} \quad , \tag{7}$$

which takes into account the effect of velocity veering and the time lag between temporal changes in the magnitude/direction of the main current and in the SPM concentration within the nepheloid layer. We use a capital Q here to distinguish between the values of the SPM flux calculated from the alternative models.

The variables in Eq. (7) are defined as follows:

$$\gamma = \begin{cases} \left[1 - \exp\left(-\frac{h}{h_d}\right)\right] & at\ h < 2H_E \\ \left[1 - \exp\left(-\frac{2H_E}{h_d}\right)\right] & at\ 2H_E < h \end{cases} \tag{8}$$

$$h_d = \frac{K}{w_s} \quad H_E = \sqrt{\frac{2K}{f}} \quad . \tag{9}$$

Here, E is the sediment pickup function, which is as yet undefined, w_S is the settling velocity of the grains, h_d measures the thickness of the nepheloid layer, γ is a shape factor, which takes into account a specific shape of the concentration profile; in the VVS model it is a piecewise exponential shape, and H_E is the Ekman scale, which can be larger ("shallow" water limit) or smaller ("deep" water limit) that the actual depth of water. Furthermore, the x and y components of the horizontal depth-integrated mass flux, $\mathbf{Q}$, are related to the SPM load m and the components of the surface current u_h, v_h, by

$$Q_x = m(u_h\Omega_r - v_h\Omega_i), \quad Q_y = m(u_h\Omega_i + v_h\Omega_r) \ . \tag{10}$$

The variables Ω_γ and Ω_i are the real and imaginary parts of the complex velocity veering function Ω, of which the exact analytical expression is given by G. I. Shapiro (personal communication, 2004). The erosion/deposition rates at a fixed location on the sea floor are computed via the divergence of the horizontal sediment fluxes and the suspension load tendency due to time lag:

$$Q_v = \frac{\partial Q_x}{\partial x} + \frac{\partial Q_y}{\partial y} + \frac{\partial_m}{\partial t} \ . \tag{11}$$

Input parameters for the VVS model are depth of water, h, surface current, $\mathbf{u}_h$, drag coefficient, C_D, Coriolis parameter, f, SPM settling velocity, w_S, and sediment pickup function, E. The SPM load, m, and horizontal mass fluxes, $\mathbf{Q}$, are obtained from the non-local balance of SPM over the entire area represented by the 2-D Eq. (7), and then the vertical flux, Q_v, is computed via Eq. (11). The vertical structure of the SPM distribution is calculated by the model using the value of depth-integrated SPM load and the non-dimensional vertical concentration profile.

2.3 Model intercalibration

In the numerical experiments, the Bailard formulation Eq. (1) has been taken as a reference model, as it is often used by numerical modellers (see Soulsby 1997). For optimum comparison of the model results in terms of the effect of velocity veering, the VVS model was calibrated to the Bailard-type model. The drag coefficient C_D in the VVS model was chosen to match the bottom shear stress of the Bailard-type model.

The pickup function, E, in the sediment component of the VVS model was calibrated in such a way that, for a steady uniform flow over a seabed covered by non-cohesive sediment (sand), it yields the same SPM load as that obtained with the Bailard-type model. From the derivation of the Bailard formulation, Eq. (1), it follows that the SPM mass flux, $\mathbf{q}_s$, can be decomposed into a product of SPM mass, m, and the transport current velocity, $\mathbf{u}_a$, so that

$$m = \frac{c_f \varepsilon_s \rho_s}{g(s-1)w_s}|\mathbf{u}_a|^3 = \frac{\varepsilon_s \rho_s \kappa^2}{g(s-1)w_s}\frac{\ln\left(\frac{a}{z_0}\right)}{\ln^3\left(\frac{h}{z_0}\right)}|\mathbf{u}_h|^3 \ . \tag{12}$$

By applying Eq. (7) to a steady and spatially uniform flow, we obtain the expression for the calibrated pick-up function for the VVS model:

$$E = \frac{w_s m}{h_d \gamma} = \frac{\rho_s \kappa^2 \varepsilon_s \ln\left(\frac{a}{z_0}\right)|\mathbf{u}_h|^3}{g(s-1)\ln^3\left(\frac{h}{z_0}\right)h_d\gamma} \ . \tag{13}$$

Finally, the (initial) change of the bed level calculated from the equation

$$\frac{\partial z_b}{\partial t} = -\frac{Q_v}{\rho_s(1-p)} \ , \tag{14}$$

where z_b is the bed level, and the erosion / deposition flux Q_v is calculated from Eq. (5) for the Bailard model and from Eq. (11) for the VVS model, after saturation to a stationary state.

3 Results

Below, the results of first experiments are discussed which illustrate the potential importance of Ekman veering for net sand-transport patterns in coastal seas.

The following numerical constants are taken (Van der Molen 2002; Soulsby 1997) for the Bailard model

$$a = 0.5\,\mathrm{m}, \quad k_s = 0.08\,\mathrm{m}, \quad s = 2.65 \ . \tag{15}$$

These parameter values are representative for micro-tidal coastal seas at midlatitudes with a sandy bottom. For the Bailard model, changes in these parameters modify only the magnitude of the transport. For the above set of parameters, Eq. (2) gives the value $c_f = 0.019$, which is similar to those used by Bailard for longshore currents (0.012–0.017). In the VVS model, the changes in both magnitude and direction may result, because these parameters occur in the turbulent diffusion coefficent K, which influences the velocity and concentration profiles, and also the nepheloid layer depth. We assume constant values for k, a and s across the whole region.

In all cases the Coriolis parameter is taken to be 10^{-4} s^{-1} ($\sim$40°), the grain density is 2650 k gm^{-3} and the porosity of the bed is 0.4. The parameters that are chosen for the model comparison are (1) depth-integrated SPM load, (2) horizontal SPM fluxes and (3) vertical SPM fluxes, resulting in erosion/deposition. The bottom shear stress is always identical in the two models due to the model intercalibration. Simulations are carried out in a domain of 100 × 100 km with a flat bottom. A series of numerical experiments has been conducted in a range of water depth of h = (10–50) m, for surface velocities between, $|\mathbf{u}_h| = 0.5$ and 1.0 m s^{-1}, and for settling velocities w_s = (0.005–0.05) m s^{-1}. Only those sets of parameters are considered that meet the Fredsøe and Deigaard criterion for suspension (namely $w_s < 0.8\ u_*$). In order to provide as similar conditions for the models as possible, the time-dependent VVS model is run until the vertical fluxes reach

their equilibrium values. In the above geometry, three cases were considered: (1) uniform, stationary flow; (2) a stationary, straight jet; and (3) a stationary meandering jet.

3.1 Uniform flow

In this case both models, by construction, produce identical SPM loads; however, the horizontal SPM mass fluxes are different due to the difference in the profiles of velocity over the vertical. In the example shown in Fig. 1, the speed of the surface current is $|\mathbf{u}_h| = 1$ ms^{-1} and the SPM settling velocity is $w_s = 0.01$ m s^{-1}. Both models give almost similar horizontal SPM fluxes in the case that water depths are 5–10 m. Deviation of the direction of the SPM flux from that of the the surface current is also negligibly small. The absolute values of SPM fluxes in deeper waters, 30–50 m, differ by a factor of 2, which is within the borders of typical discrepancy between the SPM transport models (Soulsby 1997). This discrepancy is due to the difference in the vertical profiles of velocity and suspended matter concentration used by the models. The Bailard-type model uses the law-of-wall velocity profile, while the VVS model uses a version of the Ekman spiral for the velocity profile. In the shallow water the two models converge. In the deep water the differing profiles result in the fact that the VVS model givels the transport rates slightly lower than predicted by the fourth-power-law. More importantly, the VVS model predicts that the net transport deviates to the left of the surface current by 10°–29°, due to the effect of counterclockwise velocity veering near the seabed, which is expected from classical Ekman theory. The Bailard-type model ignores this effect. As the flow is uniform, there is no divergence in the horizontal SPM fluxes, and both models give zero erosion/deposition rates.

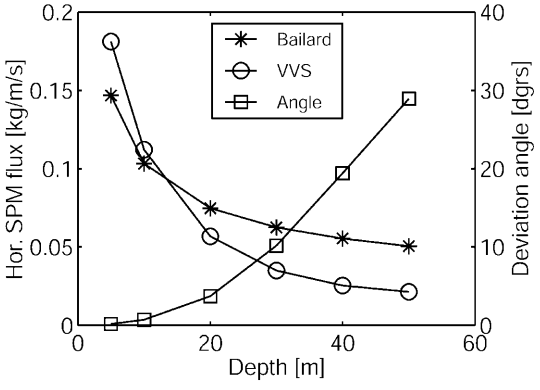

Fig. 1 Comparison of horizontal SPM fluxes by Bailard and VVS models at surface current speed, $u_h = 1$ m s^{-1}, and SPM settling velocity, $w_s = 0.01$ m s^{-1}. Also shown is the veering angle of the sediment flux with respect to the surface current in the VVS model as a function of water depth

3.2 Straight jet

The second case concerns a straight jet in a domain of 100 × 100 km with a water depth of 50 m. The jet has a width of 30 km and a maximum velocity of 0.5 m s^{-1}. In Fig. 2A the distribution of the SPM load (depth-integrated sediment concentration) across the jet is shown for sediment with a settling velocity of 0.01 m s^{-1}. Note that corresponding friction velocity is $u_* = 0.021$ m s^{-1}, and the criterion for sand suspension is satisfied. The diagrams of SPM distribution do not show significant differences between the two models. However, the distribution of the erosion–deposition flux near the bed is quite different, as is shown in Fig. 2B. The model without Ekman veering does not predict any net erosion and deposition fluxes. This is due to the fact that without veering, the sediment transport has zero horizontal divergence. On the contrary, the VVS model does show net deposition to the left of the centre of the jet, and erosion to the right of the jet. This effect is entirely due to the deviation between the direction of the SPM flux

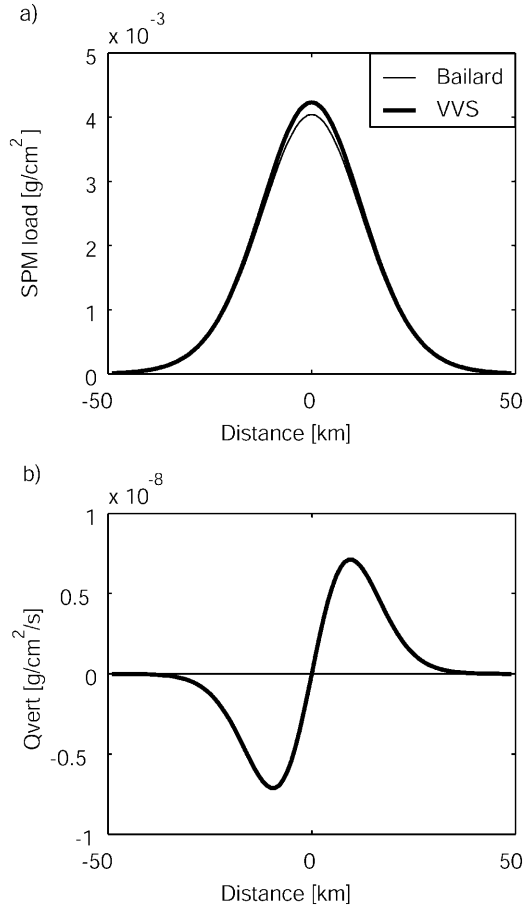

Fig. 2A, B Spatial pattern of SPM load (**A**) and erosion–deposition flux near the seabed (**B**) in the case of a straight coastal jet. *Thin curve* Bailard-type model; *thick curve* VVS model. Settling velocity is $w_s = 0.01$ m s^{-1}, depth of water $h = 50$ m, maximum surface current at the centre of the jet is $u_h = 0.5$ m s^{-1}, the Coriolis parameter is $f = 1 \times 10^{-4}$ s^{-1}

and that of the surface current, which can be seen from Table 1. At first glance, it seems surprising that grains with settling velocity as large as 0.01 ms^{-1} can be subject to a substantial veering effect, as they occupy a relatively thin suspension layer above the seabed with little veering within this layer. The physical reason is that it is the veering angle between the near-bottom current and that in the main body of water (i.e., not the veering within the suspension layer itself) that generates additional erosion/deposition fluxes. The veering angle depends on a number of parameters including the strength of the surface (or depth-averaged) current. Hence, the directions of near-bottom currents and corresponding suspended transports are different at different distances from the jet centre. This effect generates horizontal divergence/convergence of the suspended transport even when the streamlines of surface current are perfectly parallel. For both deeper (50 m) and shallower (10 m) waters the erosion and deposition patterns disappear as soon as the Coriolis effect is switched off ($f = 0$, runs 01 and 04), and the VVS model produces the same result as the Bailard model, i.e. no vertical fluxes at the seabed. Note that velocity veering is weaker in the shallower water (runs 03 and 04) than in the deeper water (runs 01 and 02). As a result of reduced velocity veering, the erosion/deposition fluxes, Q_v, are lower in the shallower water by about a factor 4 as compared to a similar flow in deep water.

Figure 3 shows how vertical SPM fluxes vary across the jet for three model cases: $H = 10$ and 50 m with velocity veering by the Coriolis force taken into account; and $H = 50$ m but no Coriolis force. Note that the pickup function is exactly the same for all three cases and is symmetric relative to the jet centre ($x = 0$). However, the gravitational settling fluxes, which are proportional to the SPM load, are different in different parts of the jet and result in different net erosion/deposition fluxes. The Coriolis force shifts the SPM cloud slightly to the left, so that the settling flux is smaller on the right of the jet, and the erosion processes prevail on the right-hand side of the jet. If the Coriolis force is ignored, the morphological effect vanishes. Note that the water depth affects only the magnitude of the bed-level change, not the shape.

Maximum deposition/erosion rates in Fig. 3 amount to about 1 mm a^{-1}, which is indeed comparable to the large-scale North Sea situation, and also to many other systems that change on a geological time scale (e.g. Van der Molen 2003). The rates in the North Sea, however, are the net (time-averaged) result of tidal action, where much larger amounts of sand are in motion at each particular moment in time

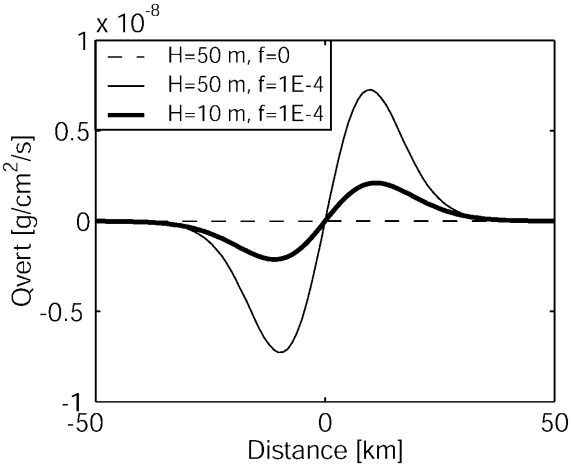

Fig. 3 Vertical SPM flux across a straight jet calculated using the VVS model, (1) for water depth $H = 50$ m with the Coriolis force (*thin solid line*); (2) for water depth $H = 50$ m without the Coriolis force (*dashed line*); and (3) for $H = 10$ m with the Coriolis force (*thick line*). Settling velocity is $w_s = 0.01$ m s^{-1}, maximum surface current at the centre of the jet is $u_h = 0.5$ m s^{-1}. The Coriolis parameter is $f = 1 \times 10^{-4}$ where applicable. Note that in the absence of veering effect, the straight jet is a non-divergent flow, and the Baliard-type model gives zero values for the vertical fluxes

3.3 Meandering coastal jet

Parameters for the meandering jet are as in the previous experiment, except for the maximum velocity in the jet (here 0.7 m s^{-1}), meander amplitude of 30 km and the meander wavelength, which is 200 km (see Fig. 4). Characteristic results of the experiments are summarised in the Table 2. The results for the distribution of the SPM load and erosion–deposition flux near the seabed are shown in Fig. 4.

For this set of experiments, the SPM loads are similar in both models. Erosion and deposition fluxes vary across the area. The maximum values of these fluxes over the whole area are shown in Table 2. For coarse sand ($w_s = 0.02$ m s^{-1}), the Bailard model gives higher erosion/deposition rates; for fine sand ($w_s = 0.005$ m s^{-1}), predicted rates are higher with the VVS model. This trend is attributed to spatial lag effects between velocity and concentration, which are accounted for in the VVS model, but not in the Bailard model. Table 2 shows that the differences between the Bailard and VVS models in

Table 1 Morphological parameters of a straight jet over a flat bottom (VVS model). In all experiments $w_s = 0.01$ m s^{-1}

Run no.	Depth of water (m)	f, s^{-1}	Maximum erosion/deposition rate (mm a^{-1})	SPM load (kg m^{-2})	Typical veering angle in the core of the flow (deg)
1	50	0	0	4.2e-2	0
2	50	1.e-4	1.1	4.2e-2	43
3	10	1.e-4	0.31	7.2e-2	8
4	10	0	0	7.2e-2	0

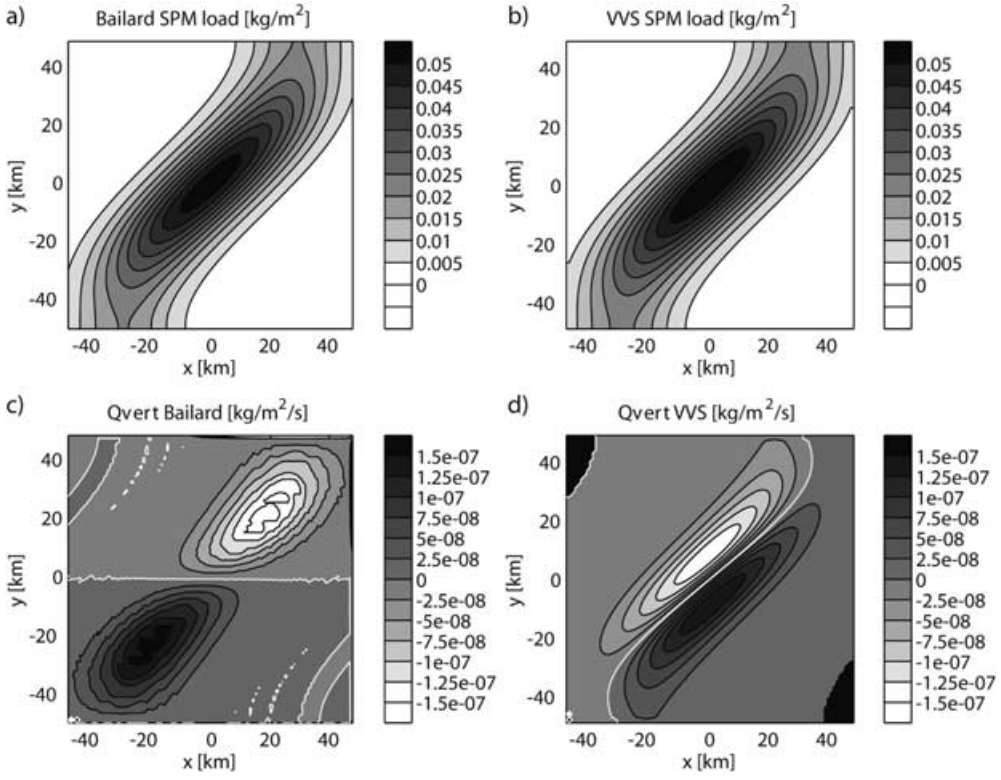

Fig. 4A–D Plan view of the meandering jet. Suspended matter load for Bailard (**A**) and VVS (**B**) models, and associated erosion/deposition patterns (**C**, **D**). In the latter two graphs, the *white lines* are zero contours. Settling velocity is $w_s = 0.02$ m s^{-1}, maximum surface current at the centre of the jet is $u_h = 0.7$ m s^{-1}, water depth is $H = 50$ m

Table 2 Model comparison for a meandering jet

Run no.	Ws, m s^{-1}	SPM load, kg m^{-2}		Maximum erosion/deposition depth, mm a^{-1}	
		Bailard	VVS	Bailard	VVS
6	0.02	5.4e-2	5.6e-2	3.4	2.2
7	0.01	1.08e-1	1.1e-1	6.7	8.3
8	0.005	2.16e-1	2.25e-1	13.4	27

the magnitudes of the key parameters are relatively small and are similar to the discrepancy between other SPM transport models. The major difference between the Bailard and VVS models is in the location of erosion and deposition areas. While the Bailard model shows erosion in the lower half of the diagram in Fig. 4 and deposition in the upper half, the VVS model predicts erosion to the right of the jet and deposition to the left. This effect is due to the veering of the SPM transport to the left of the surface current. The sediment is primarily suspended in the core of the jet and shifted by local currents along and to the left of the jet axis, where the current speed and thus the entrainment rate are lower. So the process of deposition prevails to the left of the jet. On the right-hand side of the jet the entrained sediment is eventually removed by currents but is not compensated, as there is little supply from the area of the jet farther to the right. The shift in the centre of the deposition area between the two models for this numerical run is as great as 23 km.

Surprisingly, the effect of the Coriolis force is still visible when the water depth is close to the Ekman scale. Figure 5A shows the erosion/deposition fluxes of the VVS model generated by the same jet in 20 m of water, while the maximum value of the Ekman scale in the core of the jet is 19 m. The centre of the deposition area has shifted by $L = 8$ km as compared to the no-Coriolis-force case. Figure 5B shows the veering angle of the sediment transport at each location relative to the surface current at the same location. The strength of the velocity veering effect is enhanced by the fact that the deposition area is located at the periphery of the jet, where the speed of current is lower and less turbulence is generated. Hence, the local Ekman scale is smaller, the ratio H/H_E is higher and the veering angle is greater, as shown in Fig. 5B. Away from the jet, the angle formally becomes as great as 45°; however, these distant areas do not contribute to the sediment transport as the current speeds and suspended loads are negligibly small. The two models converge if the water depth is significantly shallower than the Ekman scale, so that little veering takes place in the water column.

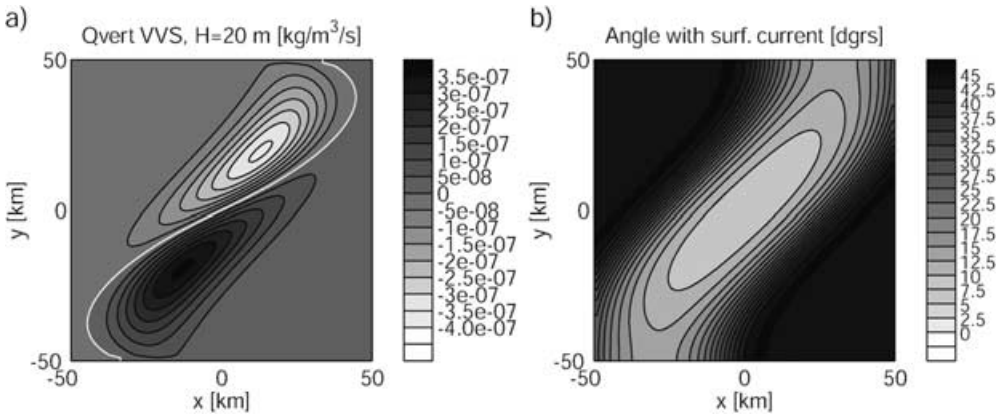

Fig. 5 **A** Vertical SPM flux at the sea bed for a meandering jet, water depth 20 m (*white line* is the zero contour). **B** Veering angle of the sediment transport relative to the surface current direction (degrees). Settling velocity is $w_s = 0.01$ m s^{-1}, maximum surface current at the centre of the jet is $u_h = 0.7$ m s^{-1}

4 Discussion

Field observations (McCave 1972) and numerical simulations (Shapiro et al. 2000) support the hypothesis that on a relatively deep shelf the velocity veering in the bottom Ekman layer causes the direction of transport of fine sediment (i.e., silt) to be generally different from the direction of the surface flow. Also, data collected on the Portuguese shelf reveal that Ekman veering of currents and their effect on transport of suspended matter is significant (Oliveira et al. 2002; Vitorino et al. 2002). In all these cases, water depths are larger than the thickness of the Ekman layer.

The present study indicates that Ekman veering and its effect on transport, erosion and deposition are also important for coarser sediment, like sand, and in shallower basins with depths comparable to the thickness of the Ekman layer (typically between 15 and 30 m).

The present version of the model is developed for SPM transport in the near-bottom layer by steady currents and is still subject to a number of limitations. The model does not account for the surface Ekman layer due to wind stress and the turbulence induced by wind waves. The model can deal with the currents with a time scale longer than the pendulum day (about 17 h at mid-latitudes), but the tidal currents cannot be accounted for yet.

In order to find support from field data for these findings, it is important to notice that in most coastal seas the water motion is rather complex: it involves contributions due to tides, surface waves, wind, internal waves etc. Thus, the data should be selected with care. Below, a dataset is discussed that was collected in a period of calm weather with quasisteady currents.

The velocity veering model results are qualitatively consistent, with regard to currents, with the data of the Long Island shelf, discussed by Niedoroda and Swift (1991). Unfortunately, they present no measured sediment fluxes. Instead, these fluxes are computed by the Grant–Madsen formulation, which does not account for Ekman veering, but uses near-bed velocities. Notice that the use of the Grant–Madsen formulation accounts for waves. Niedoroda and Swift (1991) do this to properly account for waves and because they study both the surf zone and inner shelf during both storms and fair weather conditions. Here, we are interested only in the part of the data on the shelf that corresponds to fair weather conditions. In that area and under the given circumstances, the observations reveal that waves are negligible: the current is driven by wind stress. Observations by Niedoroda and Swift (1991) have clearly demonstrated that the direction of near-bottom currents, and hence the sediment transport, deviates to the left from the surface current, in agreement with the findings of the VVS theory.

For example, in the case of a moderate downwelling situation and at a site located 3 km offshore (local depth is 19.5 m), the observed magnitude of the surface current was 0.57 m s^{-1}, with an onshore-directed velocity component of 0.06 m s^{-1}. At a distance of 1 m from the bottom the magnitude of the current was 0.15 m s^{-1} and an offshore-directed component of 0.02 m s^{-1} was measured. This implies a counterclockwise veering of the current from surface towards the bottom of 13°. The total veering of the current computed with the VVS model (assuming bottom roughness $z_0 = 0.002$ m, $w_s = 0.02$ m s^{-1}) was 15°. The difference in direction between the calculated SPM flux and that of the surface current was 13° and this flux has an offshore-directed component. These results are consistent with those of Niedoroda and Swift (1991). However, a quantitative comparison of the transport rates is not discussed here, because there were no observed transport rates to compare with and, moreover, this is beyond the aim of the present study.

5 Summary and conclusions

To verify the potential impact of velocity veering on sand transport, an intercomparison has been made of two sand-transport models. One of these neglects velocity veering due to Earth rotation effects, while the other takes it into account. The non-veering model is based on the frequently used Bailard formulation, which was previously tested against field observation elsewhere

(Van der Molen 2003). The two models use a matching set of parameters to provide identical values for the bottom stress and suspended load for a uniform steady current at any given surface velocity. The models were tested in a range of sand grain sizes 50–500 μm and current speeds up to 1 m s^{-1} for an idealised square region (100 × 100 km) of a shelf sea of constant depth. The erosion/deposition patterns and suspension load distribution were examined for three illustrative steady-state cases: uniform flow, a straight jet and a meandering jet.

In the shallow water limit (from 5 to 10 m), when both approaches are applicable, the models produce similar results. In water depth between 20 and 50 m, both the rates and the spatial distribution of erosion/deposition differ significantly between the models in both cases with a jet. This difference can be attributed to additional flux divergence due to velocity veering. Furthermore, time lags between current velocities and SPM concentration occur during the period that the concentration adjusts to the current, which are particularly significant in the case of smaller grains. The model qualitatively reproduces field observations from the Long Island shelf, as discussed by Niedoroda and Swift (1991).

While the VVS model is developed for a steady current situation, the physical mechanism behind it gives some insight into sediment transport in tidally influenced areas. It is well known that the Coriolis force influences the tidal flow, the tidal ellipses being a good signature of this effect. The consequence of this is that the currents near the bottom are always at some angle to the surface currents, and should generate additional divergence/convergence of the suspended sand transport. Rough estimates could be obtained from the present VVS model; however, more accurate calculations need to use a time-dependent version of the momentum equations.

The main conclusion is that Ekman veering affects both the magnitude and (in particular) the direction of sand transport in coastal seas. This result implies that patterns of erosion–deposition of sediment, and consequently the initial trend in morphodynamic evolution, are significantly affected by velocity veering.

Acknowledgements This work was supported by The Netherlands Council for Earth and Life Sciences (ALW), with financial aid of the Organization for Scientific Research (NWO) through grant no. 811.33.005 and by the European Union through grant INTAS 01–460.

References

Backhaus JO, Hainbucher D (1987) A finite-difference general-circulation model for shelf seas and its application to low-frequency variability on the North European Shelf. In: Nihoul JCJ, Jamart BM (eds) Three-dimensional models of marine and estuarine dynamics. Elsevier Oceanography Series 45: 221–244

Bailard JA (1981) An energetics total load sediment transport model for a plane sloping beach. J Geophys Res 86: 10938–10954

Clauser FH (1956) The turbulent boundary layer. Adv Applied Mechan 4: 1–51

De Vriend HJ, Zyserman J, Nicholson J, Roelvink JA, Péchon P, Southgate HN (1993) Medium-term 2DH coastal area modelling. Coast Eng 21: 193–224

Gerritsen H, Berentsen CWJ (1998) A modelling study of tidally induced equilibrium sand balances in the North Sea during the Holocene. Continental Shelf Res 18: 151–200

Maas LRM, Van Haren JJM (1987) Observations on the vertical structure of tidal and inertial currents in the central North Sea. J Mar Res 45: 293–318

McCave IN (1972) Transport and escape of fine-grained sediment from shelf areas. In: Swift DJP, Duane DB, Pilkey OH (eds) Shelf sediment transport: process and pattern. Dowden, Hutchinson and Ross, pp 225–244

Nicholson J, Broker I, Roelvink JA, Price D, Tanguy JM, Moreno L (1997) Intercomparison of coastal area morphodynamic models. Coast Eng 31: 97–123

Niedoroda AW, Swift DJP (1991) Shoreface processes. In: Herbich JB (ed) Handbook of coastal and ocean engineering, vol 2 Gulf Publ Co Houston pp 735–770

Oliveira A, Vitorino J, Rodrigues A, Jouanneau JM, Dias JA, Weber O (2002) Nepheloid layer dynamics in the northern Portuguese shelf. Progr Oceanogr. 52: 195–213

Pond S, Pickard GL (2001) Introductory dynamic oceanography. Butterworth Heinemann, Oxford pp 329

Prandle D (1982) The vertical structure of tidal currents and other oscillatory flows. Continental Shelf Res 1(2): 191–207

Shapiro GI, Akivis TM, Pykhov NV, Antsyferov SM (2000) Transport of fine sediment with mesoscale currents in the shelf–slope zone of the sea. Oceanology 40: 305–311

Soulsby R (1997) Dynamics of marine sands. Thomas Telford Publications, London, UK

Van der Molen J (2002) The influence of tides, wind and waves on the net sand transport in the North Sea. Continental Shelf Res (In press)

Van der Molen J (2003) Bailard's sediment transport formulation in shelf sea conditions: comparison with observations using a clustering technique. Coast Eng (In press)

Van der Molen J, de Swart HE (2001) Holocene tidal conditions and tide-induced sand transport in the southern North Sea. J Geophys Res (C) Oceans 106: 9339–9362

Van Rijn LC (1993) Principles of sediment transport in rivers, estuaries and coastal seas. Aqua Publications, Amsterdam, The Netherlands

Vitorino J, Oliveira A, Jouanneau JM, Drago T (2002) Winter dynamics on the northern Portuguese shelf, part 2. Bottom boundary layers and sediment dispersal. Progr Oceanogr 52: 155–170